Adaptive Control of a MEMS Steering Mirror for Suppression of Laser Beam Jitter

Néstor O. Pérez Arancibia, Neil Chen, Steve Gibson, and Tsu-Chin Tsao

Abstract— This paper presents an adaptive control scheme for laser-beam steering by a two-axis MEMS tilt mirror. Disturbances in the laser beam are rejected by a μ-synthesis feedback controller augmented by the adaptive control loop, which determines control gains that are optimal for the current disturbance acting on the laser beam. The adaptive loop is based on an adaptive lattice filter that implicitly identifies the disturbance statistics from real-time sensor data. Experimental results are presented to demonstrate that the adaptive controller significantly extends the disturbance-rejection bandwidth achieved by the feedback controller alone.

I. INTRODUCTION

Laser beam steering has a wide range of applications in fields such as adaptive optics, wireless communications, and manufacturing process. The control problem is to position the centroid of a laser beam at a desired location on a target plane some distance from the laser source with minimal beam motion, or jitter, in the presence of disturbances. In applications, the jitter usually is produced by vibration of the optical bench or turbulence in the atmosphere through which the beam travels. Turbulence-induced jitter may be rather broadband [1], [2], [3], [4], while vibration-induced jitter typically is composed of one or more narrow bandwidths produced by vibration modes of the structure supporting the optical system. Because the disturbance characteristics often change with time, optimal performance of a beam steering system requires an adaptive control system.

In engineering applications, lightly damped elastic modes of the beam steering mirrors also produce beam jitter. This is the case with the MEMS mirrors used in the experiment presented here. These mirrors, which are used in free-space optical communications systems, have a torsional vibration mode about each steering axis.

This paper presents a control scheme for laser beam steering in which a linear-time-invariant (LTI) feedback control loop is augmented by an adaptive control loop. The LTI feedback loop used here is a μ-synthesis controller designed to achieve two objectives: robust stabilization of the beam steering system, and a disturbance-rejection bandwidth near the maximum achievable with LTI feedback control. The adaptive loop is based on a multichannel

recursive least-squares (RLS) lattice filter that implicitly identifies the disturbance statistics in real time. The lattice filter was chosen because of its computational efficiency and numerical stability.

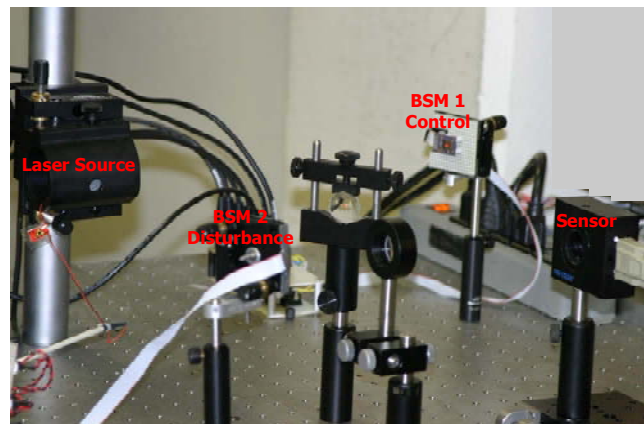## II. DESCRIPTION OF THE EXPERIMENT
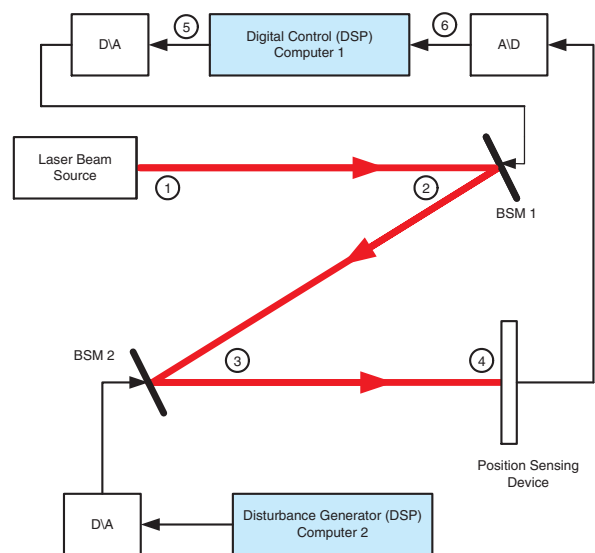

Fig. 1.   Laser beam steering experiment.

Fig. 2.   Diagram of experiment.

The experimental system is shown in the photographs and the diagram in Figs. 1–3. The main optical components in the experiment are the laser source, two MEMS beam steering mirrors, and a position sensing device (sensor).
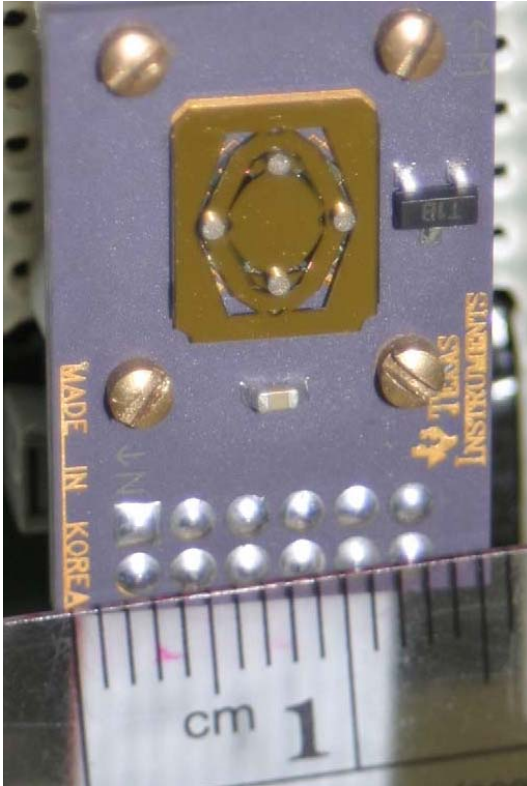
Fig. 3.   Texas Instruments MEMS Beam Steering Mirror.

commanded by the control and disturbance computers. The mirrors have a rotation range of ± 5 degrees. The reflecting area of the mirrors is 9mm^2. The optoelectronic position sensor at the end of the beam path generates two analog output voltages proportional to the two-dimensional position of the laser beam centroid. In the sensor, quad photo detectors capture the light intensity distribution, generating current outputs, which are converted to voltage and amplified by an operational amplifier. Further electronic processing of these voltage signals yields two final signals, which are the estimates of the centroid coordinates independent of light intensity.

III. SYSTEM IDENTIFICATION

Design of the feedback control system requires an open-loop model of the dynamics of the steering mirror BSM 1, and the adaptive control loop requires an estimate of the transfer function from the adaptive-control commands to the sensor outputs with the feedback loop closed. The open-loop and closed-loop transfer functions are identified by a subspace method [5], [6] using input-output data from two brief experiments in which BSM 1 was driven by white noise. After the first of these experiments, which was open-loop, the feedback controller was designed, and then the feedback loop was closed for the second experiment.

Since the sample-and-hold rate for control and filtering was 2000Hz for the experimental results presented in this paper, discrete-time models were identified for the 2000Hz rate. For identification, input-output sequences with 12,000 data points each (i.e., six seconds of data) were generated.

The disturbance actuator BSM 2 has dynamics very similar to those of BSM 1, but the control loops do not require a model of the disturbance actuator. Hence, the system identification uses data generated with BSM 2 fixed.

Experimental results showed negligible coupling between the two channels of each beam steering mirror; i.e., Axis 1 commands produced negligible rotation about Axis 2 and vice versa. Therefore, an uncoupled pair of SISO transfer functions was identified for the open-loop model of BSM 1. The subspace method identified several higher-order mirror modes, but their contribution to the input-output properties of the mirror were deemed insignificant for the purposes of the control. Therefore, a balanced truncation to two states for each mirror axis was chosen for control purposes. The frequency responses of these identified transfer functions are shown in Fig. 4.

As discussed in Section IV, the feedback controller did not couple the mirror modes, so a second uncoupled pair of SISO transfer functions was identified for closed-loop plant model used by the adaptive control loop.

The true open-loop transfer function from the BSM 1 commands to the sensor outputs (i.e., the open-loop plant) will be denoted by $P(z)$, and the identified open-loop plant model will be denoted by $\hat{P}(z)$. Similarly, the true closed-loop transfer function and identified transfer function will be denoted, respectively, by $G(z)$ and $\hat{G}(z)$.

Fig. 2 shows the path of the laser beam from the source to the sensor. After leaving the laser source, the beam reflects off the mirror BSM 1, which serves as the control actuator, then reflects of the mirror BSM 2, which adds disturbance to the beam direction, and finally goes to the sensor. Each mirror rotates about horizontal and vertical axes, denoted respectively by Axis 1 and Axis 2. The outputs of the sensor are the horizontal and vertical displacements of the centroid of the laser spot on the sensor plane. The axes for the sensor measurements are labeled Axis 2 and Axis 1, respectively, to correspond to beam deflections produced by the mirror rotations about horizontal and vertical axes. As shown in Fig. 1, there is a lens between BSM 1 and BSM 2 and another lens between BSM 2 and the sensor. These lenses focus the beam to maintain small spots on BSM 2 and the sensor.

The two sensor measurements, in the form of voltages, go to Computer 1, which has a Texas Instruments TMS320C6701 digital signal processor. This DSP runs both feedback and adaptive controllers and sends actuator commands to BSM 1. Computer 2 sends disturbance commands to BSM 2. It should be noted that the only inputs received by Computer 1, the control computer, are the two sensor measurements of the beam displacement, which are the output error in the control problem.

The commanded rotations of the beam steering mirrors are produced by electromagnetic fields with opposing directions. These fields are created by coils with currents
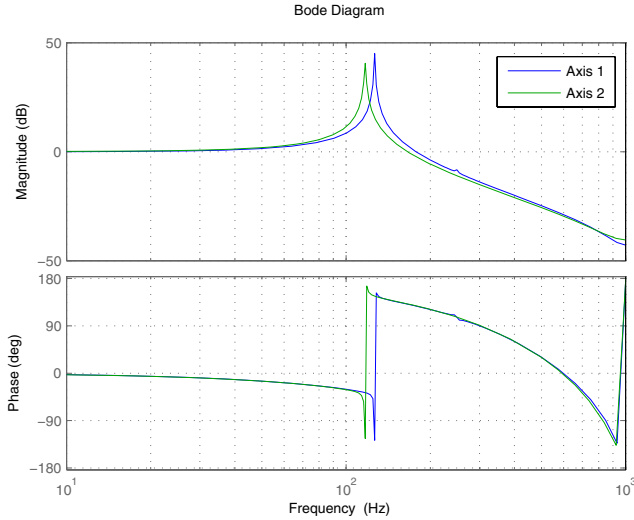
Fig. 4. Bode plots for identified model of open-loop beam steering mirror BSM 1 (control actuator). Natural frequencies: 119.4Hz (Axis 1), 126.5Hz (Axis 2).
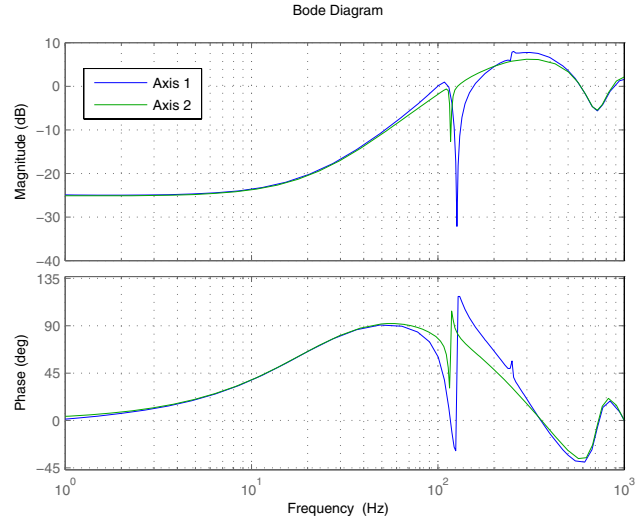

Fig. 6. Bode plots for both channels of the sensitivity transfer function $[I - \hat{P}(z)C(z)]^{-1}$.

IV. CONTROL DESIGN

A. LTI Feedback Loop

For LTI feedback control, the MATLAB μ-Analysis and Synthesis toolbox [7] was used to design a discrete-time controller with four states. The feedback system is shown in Fig. 5, where $P(z)$ is the open-loop plant and $C(z)$ is the μ-synthesis controller. This controller was designed to reject the disturbance w_0 in Fig. 5. The input u in Fig. 5 is the pair of adaptive control commands, and the output y is the pair of beam displacements measured by the sensor.
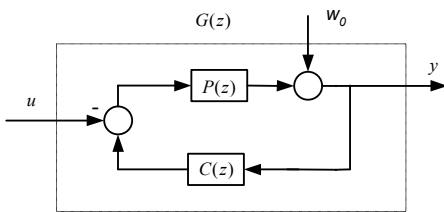

Fig. 5. Block diagram of LTI feedback control system. $P(z)$ = open-loop plant; $C(z)$ = μ-synthesis LTI feedbback controller.

Fig. 6 shows the two-channel sensitivity function for the modeled beam steering system with the LTI feedback loop closed. The input for this transfer function is a pair of output disturbances represented by the signal w_0 in Fig. 5, and the output is the pair of measured beam displacements represented by the signal y in Fig. 5. This is the pertinent sensitivity transfer function, since in the experiment, the disturbance is added to the beam after it leaves the control actuator. The sensitivity transfer function was computed using the identified open-loop plant model and the μ-synthesis feedback controller.

B. Adaptive Control Loop

In typical beam-steering applications, including adaptive optics and optical wireless communicaitons, the dynamic models of the beam steering mirrors either are known or can be determined by a one-time identification like that in Section III. The disturbance characteristics, however, depend on the atmospheric conditions in the optical path and on the excited vibration modes of the structure on which the optical systems is mounted, so that the disturbance characteristics commonly vary during operation of the beam steering system. Therefore, the adaptive control algorithm presented in this paper assumes known LTI plant dynamics but unknown disturbance dynamics. The RLS lattice filter in the adaptive control loop tracks the statistics of the disturbance and identifies gains to minimize the RMS value of the beam displacement.

Fig. 7 shows the structure of the adaptive control loop. The adaptive FIR filter $F(z)$ is the main component of the adaptive controller. As shown in the figure, the adaptive controller uses two copies of the FIR filter. The optimal filter gains are estimated in the bottom part of the block diagram in Fig. 7, and these gains are used by the FIR filter in the top part of Fig. 7.

The disturbance signal w in Fig. 7 is related to the disturbance signal w_0 in Fig. 5 by

$$w = [I - P(z)C(z)]^{-1}w_0. \qquad (1)$$

The true sensitivity transfer function $[I - P(z)C(z)]^{-1}$ is approximated closely by the transfer function in Fig. 6.

Although the LTI feedback controller consists of two uncoupled SISO controllers for the two mirror axes, the adaptive loop couples the channels by using both sensor signals as inputs to the control command for each mirror axis. The motivation for this is that, in most applicatioons,

the jitter signals in different directions are at least partially correlated. Therefore, the adaptive controller design here uses all available sensor information to suppress beam jitter in each direction. he block diagram to generate the adaptive control signal u.
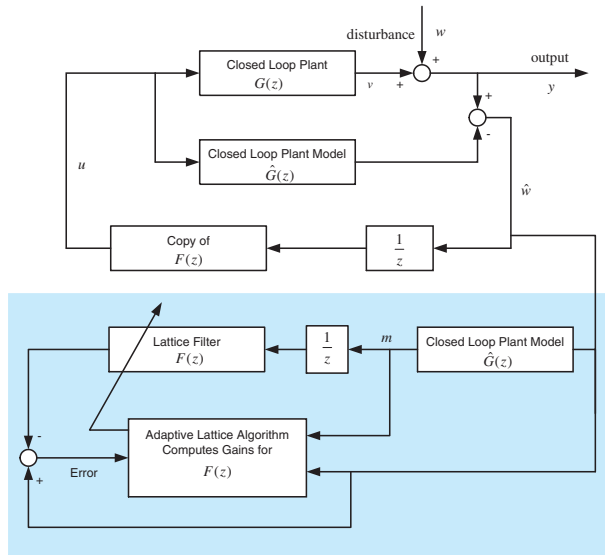

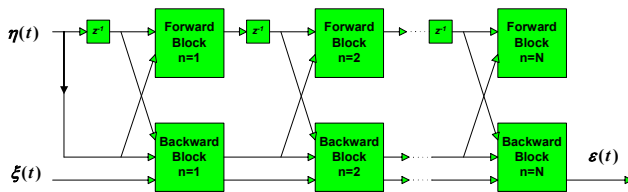Fig. 7. Block diagram of adaptive control system.

Fig. 8. Block diagram of FIR lattice filter.

Both copies of the FIR filter, as well as the RLS algorithm that estimates the optimal gains, have a lattice structure. The lattice realization of the FIR filter of order N consists of N identical stages cascaded as in Fig. 8. The details of the algorithms represented by the blocks in Fig. 8 and the RLS algorithm are beyond the scope of this paper. These algorithms are reparameterized versions of algorithms in [8]. The current parameterization of the lattice algorithms is optimized for indefinite real-time operation. The current lattice filter maintains the channel orthogonalization in [8], which is essential to numerical stability in multichannel applications, and the unwindowed characteristic of the lattice filter in [8], which is essential to rapid convergence. The inputs η and ξ to both copies of the lattice filter are constructed from the signal $\hat{w}$ in Fig. 7. The output ε of the copy of the lattice filter in the top part of Fig. 7 is the adaptive control signal.

V. EXPERIMENTAL RESULTS

Two typical sets of experimental results are shown in Figs. 9 and 10. In these experiments, the sample-and-hold rate for control and filtering was 2000Hz. The lattice-filter order $N = 16$ was used for these results. For these and other similar experiments, the performance of the adaptive loop was evaluated with several lattice-filter orders. The order 16 yielded better performance than lower orders, but orders higher than 16 yielded no further improvement.

For the experiments summarized in Fig. 9, the same disturbance command sequence was sent to each axis of the disturbance actuator BSM 2. This disturbance command signal was created by passing white noise through a fourth-order Butterworth bandpass filter with bandwidth 10Hz–50Hz. Fig. 9 shows output sequences (i.e., measured beam displacements at the sensor) for (1) an open-loop experiment, (2) an experiment with only the LTI feedback loop closed, and (3) an experiment in which the adaptive loop starts after 2000 samples (2 sec). The last two plots in Fig. 9 show the PSDs of the last 5000 points in each output sequence.

The open-loop output is just the disturbance. As the PSDs in Fig. 9 show, the disturbance contains significant power not only in the 10H–50Hz range but also around 120Hz due the the lightly damped modes of the disturbance actuator. Since the steering mirror BSM 2 is not controlled with a feeback loop, the vibration modes of this mirror are prominent in the disturbance sequences added to the laser beam.

In the experiments where the adaptive loop is closed, only the LTI feedback loop was closed for the first 2000 samples. Then the RLS lattice filter started running and ran for 50 learning steps (0.025 sec) before the adaptive control loop was closed at step 2051. Depending on the nature of the disturbance at the time when the adaptive control loop was closed, the effect of the adaptive loop on the output is seen almost immediately, as in data for Axis 1 in Fig. 9, or as much as 0.25 sec later, as in data for Axis 2 in Fig. 9.

The PSDs show that, as predicted by Fig. 6, the LTI μ-synthesis feedback loop significantly reduces the jitter below about 80Hz but has little effect beyond that. The PSDs also show that the adaptive loop yields significant jitter reduction between about 70Hz and 130Hz, thereby extending the bandwidth of the feedback loop. This extended jitter reduction in the higher frequencies accounts for the significant reduction in the RMS values of the outputs evidenced by the last 5000 samples in the time series.

Another noteworthy point in the PSDs in Fig. 9 is that both the feedback loop and the adaptive loop amplify jitter above 200Hz, and this high-frequency amplification is greater for the adaptive loop. Of course, the jitter power is so low above 200Hz that the amplification in this experiment still leaves low high-frequency power. However, it might asked whether the adaptive loop would amplify high-frequency jitter similarly if there were significant jitter power about 200Hz. The next set of experiment results answer this question.

For the experiments summarized in Fig. 10, two different

but partially correlated disturbance commands were sent to BSM 2. These two tilt command sequences are the components of the signal w_0 in Figure 5. In the experiments, this signal had the form

$$w_0 = \begin{bmatrix} 4 & 1 \\ 1 & 2 \end{bmatrix} \begin{bmatrix} v_1 \\ v_2 \end{bmatrix} \qquad (2)$$

where the sequences v_1 and v_2 were obtained by passing independent white noise sequences through bandpass filters. The bandpass filter used to generate v_1 was the sum of two Butterworth filters with bandwidths 120Hz–130Hz and 250Hz–260Hz. The filter used to generate v_2 was a Butterworth filter with bandwidth 10Hz–70Hz.

The PSDs in Fig. 10 show that, again as predicted by Fig. 6, the LTI feedback loop significantly reduces the jitter below about 80Hz, has no significant effect in the bandwidth 100Hz–130Hz, where most of the jitter power lies, but significantly amplifies the Axis-1 jitter in the bandwidth 250Hz–260Hz. In this case, as in Fig. 9, the adaptive loop significantly reduces the jitter between 70Hz and 130Hz. However, as opposed to the case in Fig. 9, the PSDs in Fig. 10 show that the adaptive loop significantly reduces the Axis-1 jitter in the bandwidth 250Hz–260Hz and only slightly amplifies the Axis-2 jitter in this bandwidth above the level to which the feedback loop raised it. The difference between the way the adaptive loop handles the 250Hz–260Hz jitter in the two axes results from the fact that the open-loop jitter in this bandwidth is approximately 20db higher for Axis 1 than for Axis 2.

Of course, the optimal FIR filter in the adaptive loop is different for the two experiments. In each case, the RLS lattice identifies the filter that is optimal for the particular disturbance. The rule that determines the frequency ranges where the adaptive loop reduces or amplifies power is that the adaptive filter generally whitens the residual-error sequence. This means accepting some power increase in bandwidths where the open-loop jitter is small to be able to achieve large reductions in the dominant jitter power.

VI. CONCLUSIONS

This paper has presented a method for adaptive suppression of jitter in laser beams. The method has been demonstrated by results from beam steering experiment employing two-axis MEMS tilt mirrors. Disturbances in the laser beam are rejected by a μ-synthesis feedback controller augmented by the adaptive control loop, which determines control gains that are optimal for the current disturbance acting on the laser beam. The adaptive loop is based on an adaptive lattice filter that implicitly identifies the disturbance statistics from real-time sensor data. Experimental results demonstrate that the adaptive controller significantly extends the disturbance rejection bandwidth achieved by the feedback controller alone. This adaptive scheme is most suited to reject jitter where the statistics of the disturbance vary from time to time due to changes in environmental conditions. The adaptive lattice filter is able to perform high order and multi-channel

RLS (recursive-least-squares) computation in real-time at high sampling rates, and RLS yields faster convergence to optimal gains than does LMS (least mean squares), which is more commonly used in adaptive disturbance-rejection applications.

REFERENCES

[1] M. C. Roggemann and B. Welsh, *Imaging through Turbulence*. New York: CRC, 1996.
[2] R. K. Tyson, *Principles of Adaptive Optics*. New York: Academic Press, 1998.
[3] B. L. Ellerbroek, "First-order performance evalution of adaptive optics systems for atmospheric turbulence compensation in extended field-of-view astronomical telescopes," *J. Opt. Soc. Am. A*, vol. 11, pp. 783–805, 1994.
[4] R. Q. Fugate and B. L. Ellerbroek et al., "Two generations of laser guide star adaptive optics experiments at the starfire optical range," *J. Opt. Soc. Am. A*, vol. 11, pp. 310–324, 1994.
[5] Y. M. Ho, G. Xu, and T. Kailath, "Fast identification of state-space models via exploitation of displacement structure," *IEEE Transactions on Automatic Control*, vol. 39, no. 10, pp. 2004–2017, October 1994.
[6] P. Van Overschee and B. De Moor, *Subspace Identification for Linear Systems*. Norwell, MA: Kluwer Academic Publishers, 1996.
[7] G. J. Balas, J. C. Doyle, K. Glover, A. Packard, and R. Smith, *μ-Analisis and Synthesis Toolbox*. Mathworks.
[8] S.-B. Jiang and J. S. Gibson, "An unwindowed multichannel lattice filter with orthogonal channels," *IEEE Transactions on Signal Processing*, vol. 43, no. 12, pp. 2831–2842, December 1995.
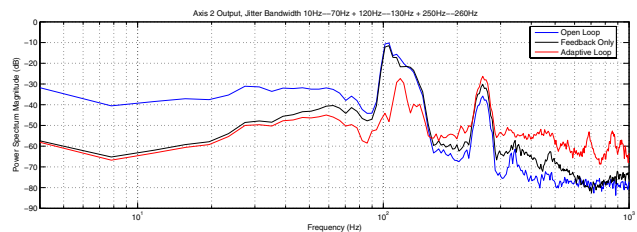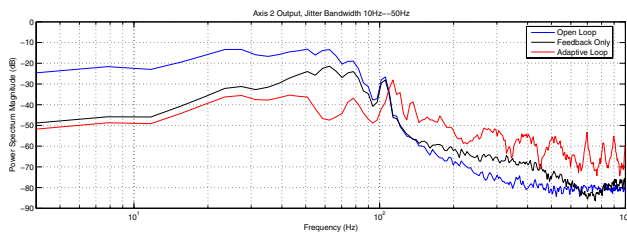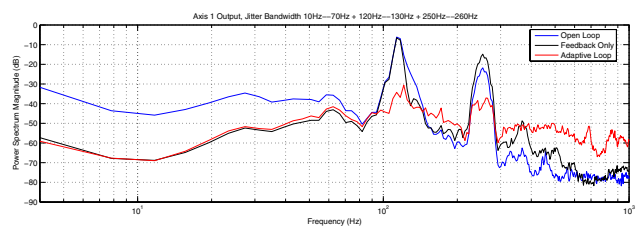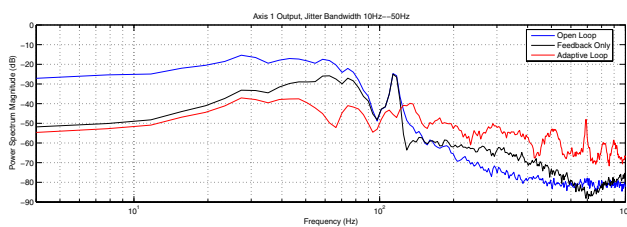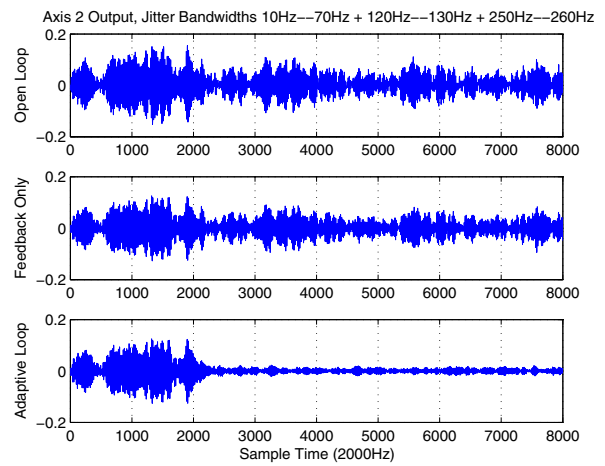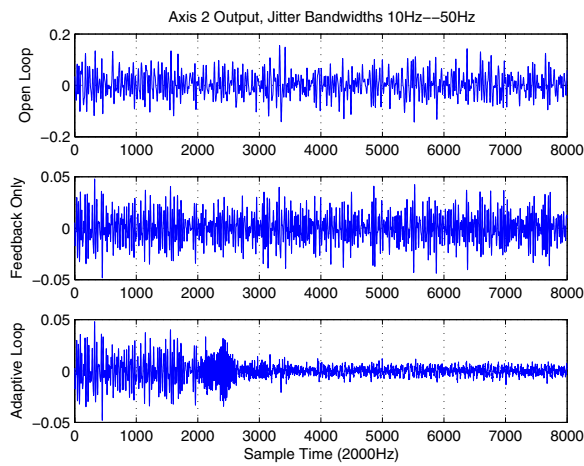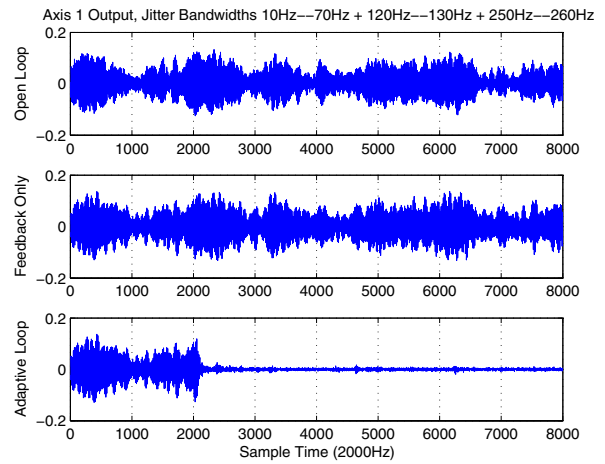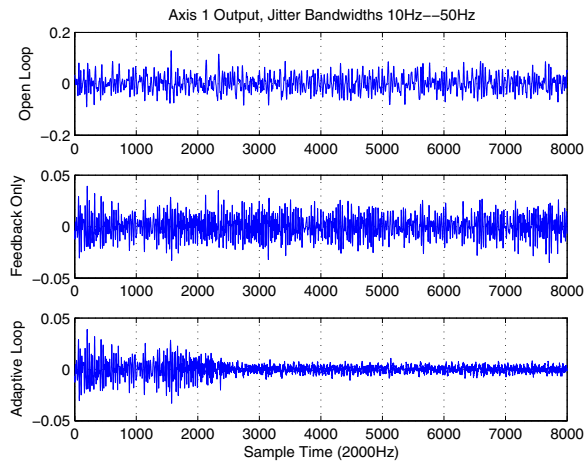
Fig. 9. Jitter bandwidth 10Hz–50Hz. Top three plots: Axis 1 outputs. Middle three plots: Axis 2 outputs. Bottom two plots: PSDs of outputs (last 5000 samples).

Fig. 10. Jitter bandwidths 10Hz–70H, 120Hz–130Hz, and 250–260Hz. Top three plots: Axis 1 outputs. Middle three plots: Axis 2 outputs. Bottom two plots: PSDs of outputs (last 5000 samples).